

# Journal of Materials Chemistry A

Accepted Manuscript



This is an *Accepted Manuscript*, which has been through the Royal Society of Chemistry peer review process and has been accepted for publication.

*Accepted Manuscripts* are published online shortly after acceptance, before technical editing, formatting and proof reading. Using this free service, authors can make their results available to the community, in citable form, before we publish the edited article. We will replace this *Accepted Manuscript* with the edited and formatted *Advance Article* as soon as it is available.

You can find more information about *Accepted Manuscripts* in the [Information for Authors](#).

Please note that technical editing may introduce minor changes to the text and/or graphics, which may alter content. The journal's standard [Terms & Conditions](#) and the [Ethical guidelines](#) still apply. In no event shall the Royal Society of Chemistry be held responsible for any errors or omissions in this *Accepted Manuscript* or any consequences arising from the use of any information it contains.

# Cu(II) nanocluster-grafted, Nb-doped TiO<sub>2</sub> as an efficient visible-light-sensitive photocatalysts based on energy-level matching between surface and bulk states

Min Liu,<sup>‡</sup> Xiaoqing Qiu,<sup>‡</sup> Kazuhito Hashimoto<sup>\*,‡,§</sup> and Masahiro Miyauchi,<sup>\*,†,||</sup>

<sup>†</sup>Department of Metallurgy and Ceramics Science, Graduate School of Science and Engineering, Tokyo Institute of Technology, 2-12-1 Ookayama, Meguro-ku, Tokyo 152-8552, Japan.

<sup>‡</sup>Research Center for Advanced Science and Technology, The University of Tokyo, 4-6-1 Komaba, Meguro-ku, Tokyo 153-8904, Japan.

<sup>§</sup>Graduate School of Engineering, The University of Tokyo, 7-3-1 Hongo, Bunkyo-ku, Tokyo 113-8656, Japan.

<sup>||</sup>Japan Science and Technology Agency (JST), ACT-C, 4-1-8 Honcho Kawaguchi, Saitama 332-0012, Japan.

Email: mmiyauchi@ceram.titech.ac.jp, hashimoto@light.t.u-tokyo.ac.jp

## Abstract

Although visible-light-sensitive photocatalysis has been reported for cupreous ion (Cu(II)) nanocluster-grafted titanium dioxide (TiO<sub>2</sub>), the visible-light absorption ( $\alpha$ ) of this system is relatively low because of its limited interfacial excitation. In the present study, we synthesized niobium (Nb)-doped TiO<sub>2</sub> grafted with Cu(II) nanoclusters and examined its capacity for visible-light absorption and photocatalytic activity for decomposing organic molecules. We speculated that the matching of energy levels between the surface Cu(II) nanoclusters and bulk-doped Nb ions would markedly increase the visible-light activity of TiO<sub>2</sub>. The doped Nb ions produced partially occupied energy levels below the conduction band of TiO<sub>2</sub> that closely matched the potential of the Cu<sup>2+</sup>/Cu<sup>+</sup> redox couple in the surface-grafted Cu(II) nanoclusters. The well-matched energy levels induced the effective transfer of photogenerated electrons from the doped Nb states to the surface-grafted Cu(II) nanoclusters, which mediated the

efficient multi-electron reduction of oxygen molecules. The prepared Cu(II)-Nb<sub>x</sub>Ti<sub>1-x</sub>O<sub>2</sub> nanocomposites exhibited a high photocatalytic reaction rate for the decomposition of 2-propanol into CO<sub>2</sub> under visible light. Our results demonstrate that efficient photocatalysts can be generated by matching the energy levels of bulk-doped ions and surface nanoclusters, which represents a strategic approach for the rational design and development of high-performance photocatalysts.

## 1. Introduction

Titanium dioxide (TiO<sub>2</sub>) has attracted considerable recent attention as an efficient photocatalyst for applications such as water splitting, organic decomposition, and solar cells.<sup>1</sup> However, because TiO<sub>2</sub> is a wide band-gap semiconductor, with band gap values of 3.2 and 3.0 eV for the anatase and rutile forms, respectively, it can only be activated under ultraviolet (UV) light irradiation, thereby limiting its practical application.<sup>2</sup> To increase the utilization of solar and indoor light sources, TiO<sub>2</sub> has been doped with various transition metal cations, such as Cr, Mn, Fe, Pb, and Cu, and anions, including N, C, and S, in an attempt to extend the light absorption capacity of TiO<sub>2</sub> into the visible light region.<sup>3</sup> Despite extensive research efforts at modifying the properties of TiO<sub>2</sub>, most doped TiO<sub>2</sub> systems remain unsuitable for practical use because their quantum efficiencies (*QEs*) under visible light are too low to support the efficient photocatalytic reactions.<sup>3,4</sup> In the case of cationic doping, the increase in visible light sensitivity is mainly caused by impurity levels in the forbidden band, which act as recombination centers for photogenerated charge carriers.<sup>2a-c</sup> In contrast, anionic doping of TiO<sub>2</sub> generally introduces isolated levels above the valence band (VB) that contain holes generated with lower oxidation power and mobility than those in the VB,<sup>4</sup> resulting in low photocatalytic performance.

Recently, the surface modification of TiO<sub>2</sub> with Cu(II) or Fe(III) nanoclusters was shown to increase its visible-light sensitivity without inducing impurity levels in the band gap.<sup>5</sup> Under visible-light irradiation, electrons in the VB of TiO<sub>2</sub> are excited to these surface nanoclusters through an interfacial charge transfer (IFCT) process.<sup>6</sup> Simultaneously, the excited electrons

are consumed in the multi-electron reduction of oxygen mediated by the nanoclusters.<sup>7</sup> Therefore, Cu(II) or Fe(III) nanocluster-grafted TiO<sub>2</sub> exhibits a high *QE* under visible light. However, the capacity of this photocatalytic system for visible-light absorption is limited because IFCT only occurs at TiO<sub>2</sub> particle/nanocluster interfaces.

Surface nanoclusters have also been demonstrated to increase the visible-light activities of doped semiconductors.<sup>5d,5f,8</sup> For example, Ti<sup>3+</sup> self-doped TiO<sub>2</sub>, which is inactive even under UV light irradiation, is converted into an efficient visible-light-sensitive photocatalyst by the surface grafting of Cu(II) or Fe(III) nanoclusters.<sup>5d</sup> Although this finding indicates that photogenerated electrons are transferred from the doped levels to the surface Cu(II) or Fe(III) nanoclusters, the *QEs* of metal-doped TiO<sub>2</sub> photocatalysts can not exceed that of Cu(II)- or Fe(III)-grafted TiO<sub>2</sub>, because the charge transfer is limited from doped levels to surface nanoclusters. Thus, efficient charge transfer between the doped levels and surface nanoclusters is critical for the photocatalytic performance of these systems. To achieve this criterion, the concept of energy level matching between the doped ions and surface-grafted nanoclusters has been recently examined using Fe(III) ion-doped and -grafted TiO<sub>2</sub> as a model system.<sup>5c</sup> The Fe(III)-doped and -grafted TiO<sub>2</sub> system exhibits a *QE* of 47.3% and a reaction rate of 0.69 μmol/h, suggesting the feasibility of this approach.

Compared with Fe(III)-based compounds, cupreous compounds have the added advantage of intrinsic anti-pathogenic properties under both dark and light conditions<sup>9</sup>, as was demonstrated for a Cu-deposited thin film of TiO<sub>2</sub>.<sup>9a</sup> Despite this advantageous characteristic, the visible-light absorption and quantum efficiencies of Cu(II)-grafted TiO<sub>2</sub> are less than those of Fe(III)-grafted TiO<sub>2</sub>.<sup>5a,5b</sup> Thus, for the development of Cu(II)-based photocatalysts that are suitable for indoor applications aimed at reducing chemical irritation or spread of infectious disease, it is necessary to markedly increase the visible-light sensitivity and photocatalytic efficiency of these materials.<sup>9</sup> Based on the concept of energy level matching, we hypothesized that this could be achieved by modifying TiO<sub>2</sub> to have similar interband energy levels as the redox potential of Cu(II) nanoclusters.

Niobium (Nb)-doped TiO<sub>2</sub> has attracted recent attention due to its intriguing electronic properties and potential applications in transparent conductive oxide, photovoltaic cells and

sensors. Theoretical and experimental studies have shown that the doping of TiO<sub>2</sub> with Nb ions generates an energy level at 0.1 to 0.2 eV below the conduction band (CB),<sup>10</sup> a value that closely matches the redox potential of Cu<sup>2+</sup>/Cu<sup>+</sup> (0.16 V vs SHE, pH=0)<sup>5a,5b</sup>. However, Nb-doped TiO<sub>2</sub> exhibits low efficiency for photocatalytic reactions because pentavalent Nb ions substitute for tetravalent Ti leading to the bulk formation of Ti<sup>3+</sup> species that serve as recombination centers.<sup>10,5d</sup> Instead, Cu(II) nanocluster-grafted (Cu(II)-TiO<sub>2</sub>) can increase its visible-light activity without introduction of impurity levels in the band gap. However, the visible-light absorption of Cu(II)-TiO<sub>2</sub> is limited because IFCT proceeds only at the bulk/nanocluster interface.

In the present study, we investigated the coupling of the bulk doping of Nb ions and surface grafting of Cu(II) clusters on TiO<sub>2</sub>. We speculated that under the visible light irradiation, excited electrons in the doped Nb levels would transfer to the Cu(II) nanoclusters owing to their similar energy levels (Figure 1), thereby increasing the visible-light sensitivity and *QE* of TiO<sub>2</sub> photocatalysts.

## 2. Experimental Section

**2.1 Synthesis of Nb<sub>x</sub>Ti<sub>1-x</sub>O<sub>2</sub>.** Nb-doped TiO<sub>2</sub> (Nb<sub>x</sub>Ti<sub>1-x</sub>O<sub>2</sub>) nanocomposites were prepared using a simple impregnation method with commercial TiO<sub>2</sub> (rutile phase, 15-nm grain size, 90 m<sup>2</sup>/g specific surface area; MT-150A, Tayca Co.) as the starting material.<sup>5c</sup> In a typical synthesis, 1.5 g TiO<sub>2</sub> powder was mixed with 10 mL ethanol to form a TiO<sub>2</sub> suspension, to which niobium(V) chloride (NbCl<sub>5</sub>, Wako, 95%) added as the source of Nb at a weight fraction to TiO<sub>2</sub> of 0.1%. The resulting suspension was stirred for 0.5 h in a vial reactor and was then dried at room temperature. The obtained residue was calcined at 950 °C for 3 h to form Nb<sub>x</sub>Ti<sub>1-x</sub>O<sub>2</sub> which was then further treated with a 6 M HCl aqueous solution at 90 °C for 3 h under stirring. The products were filtered through a 0.025-μm membrane filter (Millipore) and then washed with sufficient amounts of distilled water. Nb<sub>x</sub>Ti<sub>1-x</sub>O<sub>2</sub> was obtained as a clear powder and was dried at 110 °C for 24 h before being ground into a fine powder using an agate mortar and pestle for the preparation of Cu(II) nanocluster-grafted Nb<sub>x</sub>Ti<sub>1-x</sub>O<sub>2</sub> (Cu(II)-Nb<sub>x</sub>Ti<sub>1-x</sub>O<sub>2</sub>) nanocomposites. Pure TiO<sub>2</sub> was obtained using the same annealing and

acid treatment process without adding  $\text{NbCl}_5$  solution, and was used to prepare  $\text{Cu(II)-TiO}_2$  nanocomposites.

**2.2 Modification of  $\text{Nb}_x\text{Ti}_{1-x}\text{O}_2$  with  $\text{Cu(II)}$  Nanoclusters.** The grafting of  $\text{Cu(II)}$  nanoclusters onto  $\text{Nb}_x\text{Ti}_{1-x}\text{O}_2$  was performed using an impregnation method.<sup>5a,5b</sup> Briefly, 1 g  $\text{Nb}_x\text{Ti}_{1-x}\text{O}_2$  powder was dispersed in 10 mL distilled water and  $\text{CuCl}_2 \cdot 2\text{H}_2\text{O}$  (Wako, 99.9%) was then added to the  $\text{TiO}_2$  suspension as a source of Cu. The weight fraction of Cu relative to  $\text{TiO}_2$  was set to 0.1%. The resulting suspension was heated at 90 °C under stirred for 1 h in a vial reactor. The products were filtered through a 0.025- $\mu\text{m}$  membrane filter (Millipore) and then washed with sufficient amounts of distilled water. The obtained residue was dried at 110 °C for 24 h and subsequently ground into a fine powder using an agate mortar and pestle.  $\text{Cu(II)-TiO}_2$  was also prepared by the same impregnation method.

**2.3 Sample Characterizations.** The structural characteristics of the prepared nanocomposites were measured by powder X-ray diffraction (XRD) at room temperature on a Rigaku D/MAX25000 diffractometer with a copper target ( $\lambda=1.54056 \text{ \AA}$ ). Electron spin resonance (ESR) spectra were recorded on a Bruker ESP350E spectrometer. Elemental analyses of the samples were performed using an inductively coupled plasma-atomic emission spectrometer (ICP-AES; P-4010, Hitachi). UV–visible absorption spectra were obtained by the diffuse reflection method using a UV-2550 spectrometer (Shimadzu). The morphologies of the prepared  $\text{Nb}_x\text{Ti}_{1-x}\text{O}_2$  nanocomposites were investigated by scanning electron microscopy (SEM) using a Hitachi SU-8000 apparatus. The specific surface areas of the samples were determined from the nitrogen absorption data at liquid nitrogen temperature using the Barrett–Emmett–Teller (BET) technique. The samples were degassed at 200 °C and the pressure was kept below 100 mTorr for a minimum of 2 h prior to analysis using a Micromeritics VacPrep 061 instrument. Surface compositions and valence band X-ray photoelectron spectra were studied by X-ray photoelectron spectroscopy (XPS; model 5600, Perkin-Elmer). The binding energy data were calibrated with reference to the C 1s signal at 284.5 eV.

**2.4 Evaluation of Photocatalytic Properties.** The photocatalytic activities of the prepared nanocomposites were evaluated by monitoring the decomposition of gaseous 2-propanol (IPA)

under visible-light irradiation. A Xe lamp (LA-251Xe, Hayashi Tokei) equipped with L-42, B-47, and C-40C glass filters (Asahi Techno-Glass) was used as a source of visible light (420–530 nm, 1 mW/cm<sup>2</sup>). Light intensity was measured using a spectrum-radiometer (USR-45D, Ushio Co.) and was adjusted to 1 mW/cm<sup>2</sup>. A 500-mL cylindrical glass vessel was used as the photocatalysis reactor. To perform the photocatalytic experiments, 300 mg photocatalyst powder was evenly spread on the bottom of a circular glass dish (area of 5.5 cm<sup>2</sup>) that was mounted in the middle of the vessel reactor. The vessel was sealed with a rubber O-ring and a quartz cover, evacuated, and filled with fresh synthetic air. To eliminate organic contaminants on the sample surface, the vessel was illuminated with a Xe lamp (LA-251Xe) until the CO<sub>2</sub> generation rate was less than 0.02 μmol/day. The vessel was then evacuated and refilled with fresh synthetic air. The pressure inside the vessel was kept at ~1 atm. To begin the photocatalytic measurement, 300 ppmv (~6 μmol) of gaseous IPA was injected into the vessel, which was then incubated in the dark for 12 h to achieve the adsorption/desorption equilibrium of IPA on the photocatalyst surfaces. During this period, the IPA concentration first decreased and then remained constant, demonstrating that adsorption/desorption equilibrium had been reached. During the equilibration process, no acetone or CO<sub>2</sub> were detected, demonstrating that the IPA molecules were not decomposed by the photocatalysts under dark conditions. The vessel was then irradiated with light, and 1-mL gaseous samples were periodically extracted from the reaction vessel to measure the concentrations of IPA, acetone, and CO<sub>2</sub> using a gas chromatograph (model GC-8A; Shimadzu Co., Ltd.).

### 3. Results and Discussion

Nb<sub>x</sub>Ti<sub>1-x</sub>O<sub>2</sub> nanocomposites were prepared by a simple impregnation method and heat treatment using commercial rutile TiO<sub>2</sub> and NbCl<sub>5</sub> as starting materials. The total amount of Nb in the prepared samples was measured by ICP-AES and was found to be nearly equal to the initial value used in the preparation process (Table S1). The grafting of Cu(II) nanoclusters onto Nb<sub>x</sub>Ti<sub>1-x</sub>O<sub>2</sub> was performed by a simple impregnation method.<sup>5</sup> XRD

analysis showed that the prepared samples maintained a pure rutile  $\text{TiO}_2$  crystalline structure (JCPDS card No. 21-1276) after Nb doping or surface grafting of Cu(II) nanoclusters (Figure 2a and S1), and an aggregated  $\text{Nb}_2\text{O}_5$  phase was not detected at any of the examined doping concentrations (Figure S1). Notably, the diffraction peaks of the Nb-doped samples,  $\text{Nb}_x\text{Ti}_{1-x}\text{O}_2$  and  $\text{Cu(II)-Nb}_x\text{Ti}_{1-x}\text{O}_2$ , were shifted towards smaller angles compared with that of the undoped sample (Figure 2b). This finding indicates that Nb was substitutionally introduced into the  $\text{TiO}_2$  lattice at the Ti site, as the ionic radii of  $\text{Nb}^{5+}$  and  $\text{Nb}^{4+}$ , which are 0.69 and 0.74 Å, respectively, are larger than the 0.68 Å radius of  $\text{Ti}^{4+}$ .<sup>11,12</sup>

The morphologies of the prepared nanocomposites were examined by SEM (Figure 3 and S2), which revealed that all samples were composed of uniformly distributed nanoparticles with an average grain size of approximately 200 nm. Introduction of Cu(II) nanoclusters on the  $\text{TiO}_2$  surface as well as the doping of Nb into the  $\text{TiO}_2$  lattice did not change the morphology or particle size of the obtained  $\text{Cu(II)-Nb}_x\text{Ti}_{1-x}\text{O}_2$  samples. Therefore, the effects of morphology and particle size on photocatalytic activity can be excluded in the present study.<sup>13</sup> A TEM image clearly shows that the Cu(II) clusters, in the size of ~2 nm, are well dispersed on the surface of  $\text{Nb}_x\text{Ti}_{1-x}\text{O}_2$  particles (Figure S3). The good attachment of Cu(II) clusters to the  $\text{Nb}_x\text{Ti}_{1-x}\text{O}_2$  surfaces was observed from the corresponding high-resolution TEM (HRTEM) image. Point analysis of energy dispersive X-ray spectroscopy (EDS, Figure S3c) and surface analysis of XPS (Figure S4) proved that these clusters consist of copper compound. Further, BET surface area analysis revealed that the introduction of Nb and Cu(II) ions did not alter the surface area of  $\text{TiO}_2$  (Table S2).

The surface composition and elemental chemical states of the prepared nanocomposites were examined by XPS (Figure 4, S4 and S5). For bare  $\text{TiO}_2$ , only Ti and O were detected. The additional peaks associated with Nb were clearly observed in the spectrum of  $\text{Nb}_x\text{Ti}_{1-x}\text{O}_2$ , indicating that Nb ions were successfully introduced into the  $\text{TiO}_2$  lattice (Figure S4). For  $\text{Cu(II)-Nb}_x\text{Ti}_{1-x}\text{O}_2$ , a signal attributable to Cu was clearly detected, confirming that Cu(II) nanoclusters were grafted on the  $\text{TiO}_2$  surface (Figure S4).

Figures 4a and 4b show the Ti 2p and O 1s core-level spectra, respectively, of the nanocomposite samples. No obvious differences between the chemical states of elemental Ti



and O were observed,<sup>14</sup> demonstrating that neither the grafted Cu(II) nanoclusters nor doped Nb ions affected the bonding structure between titanium and oxygen. Further, no shoulders associated with  $Ti^{3+}$  were observed in the Ti 2p core-level spectra (Figure 4a and Figure S5), indicating that the density of  $Ti^{3+}$  was below the detection limit of the XPS analysis. The low density of  $Ti^{3+}$  in  $Nb_xTi_{1-x}O_2$  was confirmed by ESR analysis (Figure S6). Hitosugi et al.<sup>15a</sup> studied the microstructure of  $Nb^{5+}$ -doped  $TiO_2$  using XPS and found that the incorporation of  $Nb^{5+}$  into the  $TiO_2$  lattice resulted in the formation of minor  $Ti^{3+}$  components that maintain the charge balance. However, their XPS results also indicated that  $Nb^{5+}$  is reduced to  $Nb^{4+}$  under high annealing temperatures. Consistent with this finding, Khoviv et al.<sup>15b</sup> also showed that doped Nb ions in  $TiO_2$  mainly existed as  $Nb^{4+}$  after high temperature treatment.<sup>15b</sup> The formation of  $Nb^{4+}$  would not induce the generation of  $Ti^{3+}$  species.<sup>15,16</sup>

Figure 4c shows the Nb 3d core-level XPS spectra of the nanocomposite samples. For  $Nb_xTi_{1-x}O_2$  and Cu(II)- $Nb_xTi_{1-x}O_2$ , well-defined photoelectron signals located at 206.5 and 209.3 eV were observed in the obtained spectra, whereas no feature was observed in the spectrum of the undoped sample, indicating that Nb was successfully doped into  $TiO_2$  and was presented in the  $Nb^{4+}$  oxidation state.<sup>15</sup> In addition, the Nb signals in  $Nb_2O_5$  and physical mixed  $TiO_2$  and  $Nb_2O_5$  located at 207.5 and 210.4 eV (Figure S7), indicating  $Nb^{5+}$  was not detected in  $Nb_xTi_{1-x}O_2$  samples. Some previous reports indicated that the Nb doped  $TiO_2$  sample is possible to show  $Nb^{4+}$  in bulk and  $Nb^{5+}$  on the surface because of the aggregation of Nb on the surface.<sup>15b,17</sup> Our XRD data clearly demonstrated the single rutile phase of the obtained  $Nb_xTi_{1-x}O_2$  samples, revealing the well distribution of Nb in bulk  $TiO_2$ . Thus, the  $Nb^{5+}$  could not be detected in our  $Nb_xTi_{1-x}O_2$  samples and the doped Nb was existed as  $Nb^{4+}$  in the samples. On the other hand, previous reports demonstrated that the formation of  $Nb^{5+}$  and  $Ti^{3+}$  would result in the up-shift of the energy.<sup>11c-f</sup> However, our valence band (VB) XPS data clearly showed that the value of  $Nb_xTi_{1-x}O_2$  was similar to that of pure  $TiO_2$  (Figure S8). Further, no shoulder associated with  $Ti^{3+}$  was observed in the Ti 2p core-level spectra (Figure 4a and Figure S5), revealing that the density of  $Ti^{3+}$  was below the detection limit of the XPS analysis. Based on these results, it can be safely concluded that the doped Nb was well distributed in the sample and existed as  $Nb^{4+}$  oxidation state.

After modification of  $\text{Nb}_x\text{Ti}_{1-x}\text{O}_2$  with Cu(II) nanoclusters, the Cu 2p<sub>3/2</sub> core-level XPS signal was observed at 932.3 eV (Figure 4d), a value that is consistent with the results from our previous studies that used a combination of X-ray absorption fine structure (XAFS) measurements, XPS analysis, and TEM observation to characterize the Cu(II) state in a Cu(II)-TiO<sub>2</sub> system.<sup>5a,5b</sup> Based on these analyses of local crystal structure, we confirmed that Cu(II) nanoclusters were grafted on the surface of TiO<sub>2</sub> as distorted amorphous CuO-like structures with a five-coordinated square pyramidal form and a particle size of less than 3 nm.<sup>5d</sup> Our present results indicate that the chemical state and environment of Cu(II) nanoclusters in the present Cu(II)-TiO<sub>2</sub> and Cu(II)- $\text{Nb}_x\text{Ti}_{1-x}\text{O}_2$  nanocomposites are identical to those of the previously characterized Cu(II)-TiO<sub>2</sub> system.

The light absorption properties of the prepared samples were investigated by UV-visible spectroscopy (Figure 5). The spectra presented in Figure 5a clearly show that Nb doping into TiO<sub>2</sub> increased the visible-light absorption in the range of 420 to 550 nm. In addition, the grafting of Cu(II) nanoclusters on the surface of TiO<sub>2</sub> enhanced the light absorption of the resulting nanocomposite in the 420-550 and 700-800 nm wavelength regions. The increase in the shorter wavelength region can be assigned to the IFCT of VB electrons to surface Cu(II) nanoclusters, and the longer wavelength region is attributable to the d-d transition of Cu(II).<sup>5a,5b</sup> According to the band-gap estimation using Kubelka-Munk function (Figure S9), introduction of Nb ions into the TiO<sub>2</sub> lattice does not narrow the band gap of TiO<sub>2</sub>, as Nb ions are predicted to exist as isolated states in the forbidden gap. XPS (Figure 4a) and ESR analyses (Figure S6) suggested that Ti<sup>3+</sup> ions were not presented in the  $\text{Nb}_x\text{Ti}_{1-x}\text{O}_2$  nanocomposite. On the basis of these results, the visible-light absorption of the  $\text{Nb}_x\text{Ti}_{1-x}\text{O}_2$  nanocomposite is mainly attributable to the orbital of the doped Nb<sup>4+</sup> ions.

A comparison of the difference absorption spectra of Cu(II)-TiO<sub>2</sub>,  $\text{Nb}_x\text{Ti}_{1-x}\text{O}_2$ , and Cu(II)- $\text{Nb}_x\text{Ti}_{1-x}\text{O}_2$  versus bare TiO<sub>2</sub> revealed that the grafted Cu(II) nanoclusters and doped Nb ions similarly increased the visible-light absorption of these systems between 420 to 550 nm (Figure 5b). This finding indicates that doped Nb ions and grafted Cu(II) nanoclusters have similar energy levels, and that the enhanced light absorption of Cu(II)- $\text{Nb}_x\text{Ti}_{1-x}\text{O}_2$  is mainly due to the doped Nb ions.

To specify the similar energy levels between doped Nb ions and grafted Cu(II) nanoclusters, it is necessary to examine the detailed electric structure of Nb-doped TiO<sub>2</sub>. It is generally considered that excess electrons are generated when pentavalent Nb ions are substituted for tetravalent Ti ions. The generated electrons could delocalize from Nb ions to the neighboring Ti ions, resulting in the formation of Ti<sup>3+</sup> species, which introduce donor levels below the CB of TiO<sub>2</sub>.<sup>10,18</sup> However, the localized states of Nb ions in the band gap differ between the anatase and rutile forms; in the former, doped Nb ions exist as Nb<sup>5+</sup>, because a relatively low temperature is required for the formation of the anatase structure. Thus, the excess electrons from Nb<sup>5+</sup> ions could be transferred to neighboring Ti<sup>4+</sup> ions, resulting in a shift of the Fermi level toward the CB and an enhancement of the metallic behavior of anatase TiO<sub>2</sub>.<sup>19</sup> In other words, the transfer of excess electrons from Nb<sup>5+</sup> ions to Ti<sup>4+</sup> ions induces the generation of Ti<sup>3+</sup> ions, which lead to the formation localized energy states at 0.3-0.8 eV below the CB.<sup>20</sup> In contrast to the anatase form, Nb cations appear to substitute for Ti cations in rutile TiO<sub>2</sub> and exist as Nb<sup>4+</sup>.<sup>15,16,21,22</sup> The state of Nb in rutile single crystals and single crystal thin films, and rutile polymorph particles and polymorph particle thin films has been extensively analyzed using XRD, ESR, XPS, TEM, reflection high-energy and low-energy electron diffraction (RHEED and LEED), X-ray photoelectron diffraction (XPD), and scanning tunneling microscopy (STM).<sup>16,21</sup> The results of these various analyses confirmed that Nb exists as Nb<sup>4+</sup> in rutile TiO<sub>2</sub>.<sup>16,21</sup> Investigation of the phase diagram of Ti-Nb-O also indicate that TiO<sub>2</sub> and NbO<sub>2</sub> may form a solid solution of Nb<sub>x</sub>Ti<sub>1-x</sub>O<sub>2</sub> with 0 < x < 0.85 for the normal rutile phase and x > 0.85 in a deformed rutile phase at room temperature.<sup>12a</sup> The formation of Nb<sup>4+</sup> is speculated to be due to the excess electrons are remained on the Nb ions and form donor levels in the TiO<sub>2</sub> lattice. Nb-doped rutile TiO<sub>2</sub> exhibits semiconductor behavior, rather than the metallic behavior observed in the anatase form, and its Fermi level is located in the band gap.<sup>19</sup> Theoretical and experimental studies have shown that Nb<sup>4+</sup> (4d<sup>1</sup>) energy levels lie ~0.12-0.22 eV below the bottom of the CB as a partially filled state.<sup>22</sup> These findings are consistent with recent theoretical calculations that indicate Nb would form deep states in anatase and shallow states in rutile TiO<sub>2</sub>.<sup>23</sup> Although doped Nb in rutile TiO<sub>2</sub> has also been reported to remain as Nb<sup>5+</sup> ions,<sup>24</sup> whose 4d states would overlap with the O2p VB states of TiO<sub>2</sub>, our present

UV-vis spectra, XPS, ESR, and VB XPS results (Figures 4 and 5, and Figures S4-S9) clearly indicate that doped Nb exists as  $\text{Nb}^{4+}$  in the band gap. Thus, we can conclude that the doped Nb existed as  $\text{Nb}^{4+}$  in our rutile  $\text{TiO}_2$  sample and produced a shallow energy level at  $\sim 0.12\text{-}0.22$  eV below the bottom of the CB, a value that matches the redox potential of  $\text{Cu}^{2+}/\text{Cu}^+$  (0.16 V vs SHE, pH=0).<sup>5a,5b</sup>

The photocatalytic performance of the nanocomposites prepared in the present study were evaluated by the visible-light induced decomposition of IPA, which was used as a representative gaseous volatile organic compound (VOC) and is a serious pollutant of indoor air.<sup>5</sup> IPA can be completely decomposed to  $\text{CO}_2$  and water by photocatalytic oxidation.<sup>25</sup> For the photocatalytic tests, the light intensity was set to  $1 \text{ mW}/\text{cm}^2$ , which corresponds to an illuminance of 300 lux and is comparable to the intensity of white fluorescent lights and LED lights, the wavelength of the irradiation light ranged from 400 to 530 nm (Figure S10), and the initial IPA concentration was 300 ppmv ( $\sim 6 \mu\text{mol}$ ). Under these conditions, the complete decomposition of IPA would result in a  $\text{CO}_2$  concentration of 900 ppmv ( $\sim 18 \mu\text{mol}$ ), which is three times the initial IPA concentration ( $\text{CH}_3\text{CHOHCH}_3 + 9/2 \text{ O}_2 \rightarrow 3\text{CO}_2 + 4\text{H}_2\text{O}$ ). A representative curve of the change in gas concentration during the decomposition of IPA by the  $\text{Cu(II)-Nb}_x\text{Ti}_{1-x}\text{O}_2$  sample is shown in Figure 6a. Under dark conditions, the IPA concentration initially decreased and then remained constant, demonstrating that an adsorption equilibrium had been established. In addition, acetone and  $\text{CO}_2$  were not detected, indicating that IPA was not decomposed by  $\text{Cu(II)-Nb}_x\text{Ti}_{1-x}\text{O}_2$  under these conditions. With the onset of light irradiation, the IPA concentration decreased rapidly and the amount of acetone increased sharply until reaching a peak at approximately 300 ppmv, after which, the acetone concentration started to decrease. Accompanying the decrease of acetone, the concentration of  $\text{CO}_2$  increased quickly. The observed reaction profile is consistent with the photocatalytic decomposition of IPA proceeding via the formation of acetone as an intermediate, followed by the decomposition of acetone to the final products  $\text{CO}_2$  and  $\text{H}_2\text{O}$ .<sup>25</sup> After 200 h of irradiation, the concentration of  $\text{CO}_2$  in the reaction vessel reached approximately 900 ppmv ( $\sim 18 \mu\text{mol}$ ), which was nearly 3 times the amount of the initially injected IPA (300 ppmv), indicating that IPA was completely decomposed.

Comparative studies of the photocatalytic activities of  $\text{Nb}_x\text{Ti}_{1-x}\text{O}_2$ ,  $\text{Cu(II)-TiO}_2$  and  $\text{Cu(II)-Nb}_x\text{Ti}_{1-x}\text{O}_2$  samples under the same visible light source are shown in Figure 6b. After the doping of Nb ions into  $\text{Cu(II)-TiO}_2$ , the generated  $\text{Nb}_x\text{Ti}_{1-x}\text{O}_2$  nanocomposite exhibited visible-light sensitivity (Figure 5), but had relatively low photocatalytic performance, because the photogenerated charge carriers were not efficiently separated and transferred to the surface.<sup>3</sup> The  $\text{Cu(II)-TiO}_2$  nanocomposites exhibited high visible-light activity, owing to the IFCT from the VB of  $\text{TiO}_2$  to the surface  $\text{Cu(II)}$  nanoclusters and the efficient multi-electron reduction of oxygen by these nanoclusters.<sup>5-7</sup> Irie et al.<sup>5b</sup> investigated the role of  $\text{Cu(II)}$  nanoclusters in electron-trapping by performing *in situ* XAFS analysis under visible light in the presence of IPA and absence of oxygen and found that  $\text{Cu(I)}$  was generated under these conditions, but was converted back to  $\text{Cu(II)}$  upon exposure to oxygen. However, theoretical and experimental studies have revealed that the doping of Nb into  $\text{TiO}_2$  induces the formation of an energy level approximately 0.12-0.22 eV below the CB,<sup>22</sup> which is within the range of the reported redox potential of  $\text{Cu}^{2+}/\text{Cu}^+$ , 0.16 V (vs. SHE, pH=0).<sup>5a,b</sup> These results indicate that grafted  $\text{Cu(II)}$  nanoclusters and doped Nb ions have closely matched energy levels. The enhanced photocatalytic performance of  $\text{Cu(II)-Nb}_x\text{Ti}_{1-x}\text{O}_2$  compared with those of  $\text{Cu(II)-TiO}_2$  and  $\text{Nb}_x\text{Ti}_{1-x}\text{O}_2$  demonstrates that efficient energy level matching was achieved between the grafted  $\text{Cu(II)}$  nanoclusters and doped Nb ions. Based on the observed photocatalytic activities of the prepared photocatalysts, the  $QE$  for  $\text{CO}_2$  generation was calculated using the following equation:  $QE = R_p^r / R_p^a = 6R_{\text{CO}_2} / R_p^a$ , where  $R_p^r$  is the reaction rate of photons involved in  $\text{CO}_2$  generation,  $R_{\text{CO}_2}$  is the  $\text{CO}_2$  generation rate, and  $R_p^a$  is the absorption rate of incident photons. The details of this calculation are described in the literature<sup>5b</sup> and Supporting Information (Figure S11), and the data used in the calculations are summarized in Table 1. Under the same light irradiation conditions, the  $\text{Nb}_x\text{Ti}_{1-x}\text{O}_2$  sample exhibited a high absorption rate of incident photons, but a low  $\text{CO}_2$  generation rate of only 0.015  $\mu\text{mol/h}$ , indicating that this photocatalyst has a low charge separation efficiency. Although the  $\text{Cu(II)-TiO}_2$  nanocomposites displayed a high  $QE$  (27.7%), indicating that efficient IFCT and multi-electron reduction reaction proceeded on the surface,<sup>5-7</sup> the visible-light absorption rate of this material was relatively low and can be attributed to the

limited light absorption by the IFCT process (Table 1). Interestingly, the grafting of Cu(II) nanoclusters onto the surface of  $\text{Nb}_x\text{Ti}_{1-x}\text{O}_2$  resulted in strong visible-light absorption by the synthesized Cu(II)- $\text{Nb}_x\text{Ti}_{1-x}\text{O}_2$  nanocomposite, which also exhibited a high  $QE$  of 25.3%. The high reaction rate of Cu(II)- $\text{Nb}_x\text{Ti}_{1-x}\text{O}_2$  is due to the efficient light absorption by doped Nb ions and electron transfer between the doped Nb and surface-grafted Cu(II) nanoclusters, as well as the efficient multi-electron reduction of oxygen on the surface Cu(II) nanoclusters.<sup>5-7</sup> The  $QE$  of Cu(II)- $\text{Nb}_x\text{Ti}_{1-x}\text{O}_2$  is markedly higher than that of Cu(II)-grafted,  $\text{Ti}^{3+}$  self-doped  $\text{TiO}_2$ ,<sup>5d</sup> indicating that efficient charge transfer proceeds between the dopants and surface Cu(II) nanoclusters because of the similar energy levels. Due to these excellent properties, the Cu(II)- $\text{Nb}_x\text{Ti}_{1-x}\text{O}_2$  nanocomposites exhibited a  $\text{CO}_2$  generation rate of 0.20  $\mu\text{mol/h}$ , which is much higher than those of  $\text{Nb}_x\text{Ti}_{1-x}\text{O}_2$  and Cu(II)- $\text{TiO}_2$  under the same visible-light irradiation conditions.

We also investigated the photocatalytic activities of  $\text{TiO}_2$  modified with Cu(II) surface nanoclusters and various metal ions as dopants (Figure 6c). In addition to Nb dopants, we also have checked the photocatalytic performances of Fe and W doped  $\text{TiO}_2$  with various doping densities (Figure S12). The results showed that 0.1 wt% was also the optimal amount for Fe and W doped  $\text{TiO}_2$ . The synthesized nanocomposites were all single phases of the rutile  $\text{TiO}_2$  crystal structure. Among the examined metal dopants, Cu(II)- $\text{Nb}_x\text{Ti}_{1-x}\text{O}_2$  nanocomposites exhibited the best performance, indicating well energy level matching was occurred between doped Nb ions and grafted Cu(II) nanoclusters. Further, the visible-light activity of Cu(II)- $\text{Nb}_x\text{Ti}_{1-x}\text{O}_2$  was superior to that of  $\text{TiO}_{2-x}\text{N}_x$ , which is widely recognized as one of the most efficient visible-light photocatalysts reported to date (Figure 6d and Table 1).<sup>3a</sup>  $\text{TiO}_{2-x}\text{N}_x$  exhibited a rather low  $QE$  of 3.9% and required a much longer incubation period, over 300 h, to completely decompose the gaseous IPA. The low activity of this system originates from the lower oxidation power of the photogenerated holes in the nitrogen levels than those in the VB.<sup>4</sup>

Finally, we attempted to optimize the experimental conditions for enhancing the activity and found that 0.1 wt% was the optimal amount for both doped Nb and surface-grafted Cu(II) nanoclusters (Figure S13 and S14). A good junction between the surface-grafted Cu(II)

nanoclusters and bulk-doped Nb ions was also critical for the efficient charge transfer. Notably, if a thin layer was introduced between the surface Cu(II) nanoclusters and doped Nb ions (Figure S15), the visible-light activity was markedly reduced (Figure S16). The Cu(II)-Nb<sub>x</sub>Ti<sub>1-x</sub>O<sub>2</sub> sample was also very active under UV-light irradiation. Taken together, these findings suggest that Cu(II)-Nb<sub>x</sub>Ti<sub>1-x</sub>O<sub>2</sub> nanocomposites are promising visible-light-sensitive photocatalysts for practical applications.

#### 4. Conclusions

Efficient visible-light-sensitive TiO<sub>2</sub> photocatalysts were developed based on the concept of energy level matching between surface-grafted Cu(II) nanoclusters and bulk-doped Nb ions. Bulk-doped Nb ions produce energy levels below the CB of TiO<sub>2</sub>, which matches well with the redox potential of Cu<sup>2+</sup>/Cu<sup>+</sup> in surface-grafted Cu(II) nanoclusters. Both grafted Cu(II) nanoclusters and doped Nb ions induce similar increases in light absorption in the wavelength region from 420 to 550 nm. In this photocatalytic system, Ti ions were substituted for doped Nb ions that existed in the Nb<sup>4+</sup> oxidation state, which avoided the generation of Ti<sup>3+</sup> species. The doping of Nb ions enhanced the visible-light absorption of TiO<sub>2</sub>, whereas the grafting of Cu(II) nanoclusters retained the high *QE* of this system. The present Cu(II)-Nb<sub>x</sub>Ti<sub>1-x</sub>O<sub>2</sub> nanocomposites exhibited strong visible-light absorption and maintained a high *QE*, leading to high visible-light photocatalytic performance for the decomposition of gaseous organic compounds. Thus, our findings demonstrate that Cu(II)-Nb<sub>x</sub>Ti<sub>1-x</sub>O<sub>2</sub> is a suitable visible-light-sensitive photocatalyst for practical applications, and that the concept of energy level matching is an effective approach for the construction of advanced visible-light photocatalysts.

#### Acknowledgment

This work was performed under the management of the Project to Create Photocatalysts Industry for Recycling-Oriented Society supported by the New Energy and Industrial Technology Development Organization (NEDO) in Japan. This research was also supported

by the ACT-C program of the Japan Science and Technology (JST) Agency.

**Electronic supplementary information (ESI) available:** Table S1, amount of Nb in the samples derived from ICP-AES spectrophotometry. Table S2, BET surface areas of the samples. Figure S1, XRD patterns of  $\text{Nb}_x\text{Ti}_{1-x}\text{O}_2$ . Figure S2, SEM images of  $\text{Nb}_x\text{Ti}_{1-x}\text{O}_2$ . Figure S3, TEM images and EDS pattern of  $\text{Cu(II)-Nb}_x\text{Ti}_{1-x}\text{O}_2$ . Figure S4, full-scale XPS spectra of the prepared samples. Figure S5, Ti 2p core-level spectra of  $\text{Nb}_x\text{Ti}_{1-x}\text{O}_2$ . Figure S6, ESR spectra of  $\text{Nb}_x\text{Ti}_{1-x}\text{O}_2$ . Figure S7, Nb 3d core-level spectra of  $\text{Nb}_x\text{Ti}_{1-x}\text{O}_2$ ,  $\text{Nb}_2\text{O}_5$  and mixture of  $\text{Nb}_2\text{O}_5$  and  $\text{TiO}_2$ . Figure S8, Valence band XPS spectra of the samples. Figure S9, Band gap of the samples. Figure S10, light source for the visible-light irradiation. Figure S11, details of the quantum efficiency calculations. Figure S12,  $\text{CO}_2$  generation curve for  $\text{Cu(II)-Fe}_x\text{Ti}_{1-x}\text{O}_2$  and  $\text{Cu(II)-W}_x\text{Ti}_{1-x}\text{O}_2$  with different doping densities. Figures S13, comparative evaluation of  $\text{CO}_2$  generation by  $\text{Cu(II)-Nb}_x\text{Ti}_{1-x}\text{O}_2$  with different doping densities. Figure S14, comparative evaluation of  $\text{CO}_2$  generation by  $\text{Cu(II)-Nb}_x\text{Ti}_{1-x}\text{O}_2$  with different amounts of  $\text{Cu(II)}$  nanoclusters. Figure S15, preparation of  $\text{Cu(II)-TiO}_2@\text{Nb}_x\text{Ti}_{1-x}\text{O}_2$ . Figure S16,  $\text{CO}_2$  generation curve for the  $\text{Cu(II)-Nb}_x\text{Ti}_{1-x}\text{O}_2$  and  $\text{Cu(II)-TiO}_2@\text{Nb}_x\text{Ti}_{1-x}\text{O}_2$  samples.

## References

- (a) A. Fujishima, K. Honda, *Nature* 1972, **238**, 37-38. (b) T. L. Thompson, J. T. Yates, *Chem. Rev.* 2006, **106**, 4428-4453; (c) B. O'Regan, and M. Gratzel, *Nature* 1991, 353, 737-740; (d) R. Liu, P. Wang, X. F. Wang, H. G. Yu, J. G. Yu, *J. Phys. Chem. C* 2012, **116**, 17721-17728; (e) P. Wang, J. Wang, X. F. Wang, H. G. Yu, J. G. Yu, *Appl. Catal. B* 2013, **132-133**, 452-459.
- (a) M. R. Hoffmann, S. T. Martin, W. Y. Choi, and D. W. Bahnemann, *Chem. Rev.* 1995, **95**, 69-96; (b) X. Chen, and S. S. Mao, *Chem. Rev.* 2007, **107**, 2891-2959; (c) X. Chen, S. Shen, L. Guo, and S. S. Mao, *Chem. Rev.* 2010, **110**, 6503-6570; (d) M. Zhong, Y. Sato, M. Kurniawan, A. Apostoluk, B. Masenelli, E. Maeda, Y. Ikuhara, J.



- J. Delaunay, *Nanotechnology* 2012, **23**, 495602; (e) M. Liu, W. M. Lu, L. Zhao, C. L. Zhou, H. L. Li, W. J. Wang, *T. Nonferr. Metal. Soc.* 2010, **20**, 2299-2302.
- 3 (a) R. Asahi, T. Morikawa, T. Ohwaki, K. Aoki, Y. Taga, *Science* 2001, **293**, 269-271; (b) D. F. Wang, J. H. Ye, T. Kako, T. Kimura, *J. Phys. Chem. B* 2006, **110**, 15824-15830; (c) A. Kudo, R. Niishiro, A. Iwase, H. Kato, *Chem. Phys.* 2007, **339**, 104-110; (d) H. Kato, A. Kudo, *J. Phys. Chem. B* 2002, **106**, 5029-5034; (e) H. Irie, Y. Maruyama, K. Hashimoto, *J. Phys. Chem. C* 2007, **111**, 1847-1852; (f) T. H. Xie, X. Y. Sun, J. Lin, *J. Phys. Chem. C* 2008, **112**, 9753-9759; (g) M. Miyauchi, M. Takashio, H. Tobimatsu, *Langmuir* 2004, **20**, 232-236; (h) X. Y. Sun, J. Lin, *J. Phys. Chem. C* **2009**, *113*, 4970-4975; (i) M. Mrowetz, W. Balcerski, A. J. Colussi, M. R. Hoffmann, *J. Phys. Chem. B* 2004, **108**, 17269-17273; (j) M. Liu, L. Piao, S. Ju, W. Lu, L. Zhao, C. Zhou, W. Wang, *Mater. Lett.* 2010, **64**, 1204-1207.
- 4 (a) H. Irie, Y. Watanabe, and K. Hashimoto, *J. Phys. Chem. B* 2003, **107**, 5483-5486; (b) M. Miyauchi, A. Ikezawa, H. Tobimatsu, H. Irie, K. Hashimoto, *Phys. Chem. Chem. Phys.* 2004, **6**, 865-870.
- 5 (a) H. Irie, S. Miura, K. Kamiya, and K. Hashimoto, *Chem. Phys. Lett.* 2008, **457**, 202-205; (b) H. Irie, K. Kamiya, T. Shibanuma, S. Miura, D. A. Tryk, T. Yokoyama, and K. Hashimoto, *J. Phys. Chem. C* 2009, **113**, 10761-10766; (c) H. Yu, H. Irie, Y. Shimodaira, Y. Hosogi, Y. Kuroda, M. Miyauchi, and K. Hashimoto, *J. Phys. Chem. C* 2010, **114**, 16481-16487; (d) M. Liu, X. Q. Qiu, M. Miyauchi, and K. Hashimoto, *Chem. Mater.* 2011, **23**, 5282-5286; (e) M. Liu, X. Q. Qiu, M. Miyauchi, and K. Hashimoto, *J. Am. Chem. Soc.* 2013, **135**, 10064-10072; (f) X. Q. Qiu, M. Miyauchi, H. Yu, H. Irie, K. Hashimoto, *J. Am. Chem. Soc.* 2010, **132**, 15259-15267.
- 6 (a) C. Creutz, B. S. Brunshwig, and N. Sutin, *J. Phys. Chem. B* 2005, **109**, 10251-10260; (b) C. Creutz, B. S. Brunshwig, and N. Sutin, *J. Phys. Chem. B* 2006, **110**, 25181-25190.
- 7 (a) F. Himro, L. A. Eriksson, F. Maseras, and P. E. M. Siegbahn, *J. Am. Chem. Soc.* 2000, **122**, 8031-8036; (b) S. Goldstein, G. Czapski, R. Eldik, H. Cohen, and D. Meyerstein, *J. Phys. Chem.* 1991, **95**, 1282-1285; (c) N. Kitajima, and Y. Morooka,

- Chem. Rev.* 1994, **94**, 737-757; (d) A. P. Cole, D. E. Root, P. Mukherjee, E. I. Solomon, and T. D. P. Stack, *Science* 1996, **273**, 1848-1850; (e) Y. Nosaka, S. Takahashi, H. Sakamoto, A. Nosaka, *J. Phys. Chem. C* 2011, **115**, 21283-21290; (f) M. Nishikawa, Y. Mitani, Y. Nosaka, *J. Phys. Chem. C* 2012, **116**, 14900-14907.
8. (a) S. Anandan, M. Miyauchi, *Phys. Chem. Chem. Phys.* 2011, **13**, 14937-14945; (b) Y. Nosaka, S. Takahashi, Y. Mitani, X. Qiu, M. Miyauchi, *Appl. Catal. B* 2012, **111**, 636-640; (c) S. Anandan, M. Miyauchi, *Electrochem.* 2011, **79**, 842-844; (d) S. Anandan, N. Ohashi, M. Miyauchi, *Appl. Catal. B* 2010, **100**, 502-509.
9. (a) K. Sunada, T. Watanabe, K. Hashimoto, *Environ. Sci. Technol.* 2003, **37**, 4785-4789; (b) K. Sunada, M. Minoshima, K. Hashimoto, *J. Hazard. Mater.* 2012, **235-236**, 265-270; (c) X. Q. Qiu, M. Miyauchi, K. Sunada, M. Minoshima, M. Liu, Y. Lu, D. Li, Y. Shimodaira, Y. Hosogi, Y. Kuroda, K. Hashimoto, *ACS Nano*, 2012, **6**, 1609-1618.
- 10 (a) H. Y. Lee, J. Robertson, *J. Appl. Phys.* 2013, **113**, 213706; (b) K. K. Ghuman and C. V. Singh, *J. Phys: Condens. Mater.* 2013, **25**, 475501; (c) K. C. OK, Y. Park, K. B. Chung, J. S. Park, *J. Phys. D: Appl. Phys.* 2013, **46**, 295102; (d) K. N. Song, X. P. Han, G. S. Shao, *J. Alloy. Compd.* 2013, **551**, 118-124.
- 11 (a) J. Baumard, E. Tani, *J. Chem. Phys.* 1977, **67**, 857-860; (b) M.C. Carotta, M. Ferroni, D. Gnani, V. Guidi, M. Merli, G. Martinelli, M.C. Casale, M. Notaro, *Sens. Actuators B Chem.* 1999, **58**, 310-317; (c) Y. Furubayashi, T. Hitosugi, Y. Yamamoto, K. Inaba, G. Kinoda, Y. Hirose, T. Shimada, T. Hasegawa, *Appl. Phys. Lett.* 2005, **86**, 252101; (d) X. Lu, W. Yang, Z. Quan, T. Lin, L. Bai, L. Wang, F. Huang, and Y. Zhao, *J. Am. Chem. Soc.* 2014, **136**, 419-426; (e) T. Nikolay, L. Larina, O. Shevaleevskiy, and B. T. Ahn, *Energy Environ. Sci.* 2011, **4**, 1480-1486; (f) X. Lu, X. Mou, J. Wu, D. Zhang, L. Zhang, F. Huang, F. Xu, S. Huang, *Adv. Funct. Mater.* 2010, **20**, 509-515.
- 12 (a) K. Sakata, *J. Phys. Soc. Jpn.* 1969, **26**, 1067; (b) A. M. Ruiz, G. Dezanneau, J. Arbiol, A. Cornet, J. R. Morante, *Chem. Mater.* 2004, **16**, 862-871.
- 13 (a) H. H. Wang, C. S. Xie, W. Zhang, S. Z. Cai, Z. H. Yang, Y. H. Gui, *J. Hazard.*

- Mater.* 2007, **14**, 645-652; (b) D. Li, H. Haneda, *Chemosphere* 2003, **51**, 129-137.
14. M. Oku, K. Wagatsuma, S. Kohiki, *Phys. Chem. Chem. Phys.* 1999, **1**, 5327-5331.
15. (a) T. Hitosugi, H. Kamisaka, K. Yamashita, H. Nogawa, Y. Furubayashi, S. Nakao, N. Yamada, A. Chikamatsu, H. Kumigashira, M. Oshima, Y. Hirose, T. Shimada, T. Hasegawa, *Appl. Phys. Express* 2008, **1**, 111203; (b) D. A. khoviv, S. V. Zaytsev, V. M. Levlev, *Thin Solid Films* 2012, **520**, 4796-4799.
16. (a) P. F. Chester, *J. Appl. Phys.* 1961, **32**, 866-868; (b) P. H. Zimmerman, *Phys. Rev. B* 1973, **8**, 3917-3927.
17. L. R. Sheppard, *J. Phys. Chem. C* 2013, **117**, 3407-3413.
18. (a) P. Deak, B. Aradi, and T. Frauenheim, *Phys. Rev. B* 2011, **83**, 155207; (b) T. Yamamoto and T. Ohno, *Phys. Rev. B* 2012, **85**, 033104; (c) J. K. Yang, X. T. Zhang, C. H. Wang, P. P. Sun, L. L. Wang, B. Xia, Y. C. Liu, *Solid State Sci.* 2012, **14**, 139-144.
19. H. Kamisaka, T. Hitosugi, K. Yamashita, *J. Surf. Sci. Soc. Jpn.* 2010, **31**, 343.
20. D. C. Valentin, G. Pacchioni, A. Selloni, *J. Phys. Chem. C* 2009, **113**, 20543.
21. (a) S. A. Chambers, Y. Gao, Y. J. Kim, M. A. Henderson, S. Thevuthasan, S. Wen, K. L. Merkle, *Surf. Sci.* 1996, **365**, 625-637; (b) S. A. Chambers, Y. Gao, S. Thevuthasan, Y. Liang, N. R. Shivaparan, R. J. Smith, *J. Vac. Sci. Technol.* 1996, **14**, 1387-1394; (c) Y. Gao, S. A. Chambers, *J. Mater. Res.* 1996, **11**, 1025-1029; (d) Y. Gao, Y. Liang, S. A. Chambers, *Surf. Sci.* 1996, **348**, 17-27; (e) Y. Gao, S. Thevuthasan, D. E. McCready, *J. Gryst. Growth.* 2000, **212**, 178-190; (f) A. Sasahara, M. Tomitori, *J. Phys. Chem. C* 2013, **117**, 17680-17686; (g) M. Chiesa, M. C. Paganini, S. livraghi, E. Giamello, *Phys. Chem. Chem. Phys.* 2013, **15**, 9435; (h) Z. H. Zhang, S. Y. Wu, P. Xu, L. L. Li, S. X. Zhang, *Eur. Phys. J. Appl. Phys.* 2011, **53**, 20902.
22. (a) J. B. Goodenough, *Les oxydes des metaux de transition*, Gauthier-Villars, Paris, 1973. (b) J. Claverie, J. Verniolle, G. Campet, J. P. Doumerc, P. Hagenmuller, *Mat. Res. Bull.* 1981, **16**, 1019-1025; (c) T. Okamura, H. Okushi, *Jpn. J. Appl. Phys.* 1993, **32**, L454-L457; (d) K. A. Michalow, D. Flak, A. Heel, M. P. Wojtan, M. Rekas, T. Graule, *Environ. Sci. Pollut. Res.* 2012, **19**, 3696-3708; (e) H. O. Finklea, *Semiconductor electrodes*, Elsevier, Amsterdam, 1988, 58-61.

23. (a) H. Y. Lee, J. Robertson, *J. Appl. Phys.* 2013, **113**, 213706; (b) T. Yamamoto, T. Ohno, *Phys. Rev. B* 2012, **85**, 033104; (c) P. Deak, B. Aradi, T. Frauenheim, *Phys. Rev. B* 2011, **83**, 155207.
24. D. Morris, Y. Dou, J. Rebane, C. E. J. Mitchell, R. G. Egdell, D. S. L. Law, A. Vittadini, M. Casarin, *Phys. Rev. B* 2000, **61**, 13445-13457.
25. Y. Ohko, K. Hashimoto, A. Fujishima, *J. Phys. Chem. A* 1997, **101**, 8057-8062.

**Table 1.** Performances of the prepared photocatalysts.

Sample	TiO <sub>2-x</sub> N <sub>x</sub>	Nb <sub>x</sub> Ti <sub>1-x</sub> O <sub>2</sub>	Cu(II)-TiO <sub>2</sub>	Cu(II)-Nb <sub>x</sub> Ti <sub>1-x</sub> O <sub>2</sub>
$R_p^i$ ( <i>quanta/sec</i> )	$1.30 \times 10^{16}$	$1.30 \times 10^{16}$	$1.30 \times 10^{16}$	$1.30 \times 10^{16}$
$R_p^a$ ( <i>quanta/sec</i> )	$4.10 \times 10^{15}$	$6.53 \times 10^{14}$	$4.69 \times 10^{14}$	$7.91 \times 10^{14}$
$R_{co2}$ ( $\mu\text{mol/h}$ )	0.16	0.015	0.13	0.20
$QE$ (%)	3.9	2.3	27.7	25.3

$R_p^i$ , rate of incident photons.

$R_p^a$ , absorbed photon number.

$R_{co2}$ , CO<sub>2</sub> generation rate.

$QE$ , quantum efficiency.

**Figure captions**

**Figure 1.** Proposed photocatalytic processes for  $\text{Nb}_x\text{Ti}_{1-x}\text{O}_2$ ,  $\text{Cu(II)-TiO}_2$  and  $\text{Cu(II)-Nb}_x\text{Ti}_{1-x}\text{O}_2$ , respectively.

**Figure 2.** (a) XRD patterns of bare  $\text{TiO}_2$ ,  $\text{Cu(II)-TiO}_2$ ,  $\text{Nb}_x\text{Ti}_{1-x}\text{O}_2$ , and  $\text{Cu(II)-Nb}_x\text{Ti}_{1-x}\text{O}_2$  nanocomposites at  $x=0.1$  wt%. (b) Extended XRD patterns of the samples in (a).

**Figure 3.** SEM images of (a) bare  $\text{TiO}_2$ , (b)  $\text{Nb}_x\text{Ti}_{1-x}\text{O}_2$ , and (c)  $\text{Cu(II)-Nb}_x\text{Ti}_{1-x}\text{O}_2$ .

**Figure 4.** (a) Ti 2p, (b) O 1s (c) Nb 3d and (d) Cu 2p core-level spectra of bare  $\text{TiO}_2$ ,  $\text{Nb}_x\text{Ti}_{1-x}\text{O}_2$ , and  $\text{Cu(II)-Nb}_x\text{Ti}_{1-x}\text{O}_2$  nanocomposites at  $x=0.1$  wt%.

**Figure 5.** (a) UV-visible reflectance spectra of  $\text{TiO}_2$ ,  $\text{Cu(II)-TiO}_2$ ,  $\text{Nb}_x\text{Ti}_{1-x}\text{O}_2$  and  $\text{Cu(II)-Nb}_x\text{Ti}_{1-x}\text{O}_2$  nanocomposites. Inset shows the enlarged UV-visible reflectance spectra at the range of 400-520 nm. (b) Difference UV-vis spectra for  $\text{Cu(II)-TiO}_2$ ,  $\text{Nb}_x\text{Ti}_{1-x}\text{O}_2$  and  $\text{Cu(II)-Nb}_x\text{Ti}_{1-x}\text{O}_2$  nanocomposites at  $x=0.1$  wt% versus bare  $\text{TiO}_2$ .

**Figure 6.** (a) Representative time-dependent gas concentrations during IPA decomposition by  $\text{Cu(II)-Nb}_x\text{Ti}_{1-x}\text{O}_2$ . (b) Comparative studies of  $\text{CO}_2$  generation by bare  $\text{Nb}_x\text{Ti}_{1-x}\text{O}_2$ ,  $\text{Cu(II)-TiO}_2$ , and  $\text{Cu(II)-Nb}_x\text{Ti}_{1-x}\text{O}_2$  at  $x=0.1$  wt%. (c)  $\text{CO}_2$  generation curves for  $\text{Cu(II)-M}_x\text{Ti}_{1-x}\text{O}_2$  ( $M=\text{Nb, Fe, Ce, Mo, Ni, W, Cr, and Cu, } x=0.1$  wt%) samples under visible-light irradiation. (d)  $\text{CO}_2$  generation over bare  $\text{TiO}_2$ ,  $\text{TiO}_{2-x}\text{N}_x$ , and  $\text{Cu(II)-Nb}_x\text{Ti}_{1-x}\text{O}_2$  at  $x=0.1$  wt%.

Figure 1.

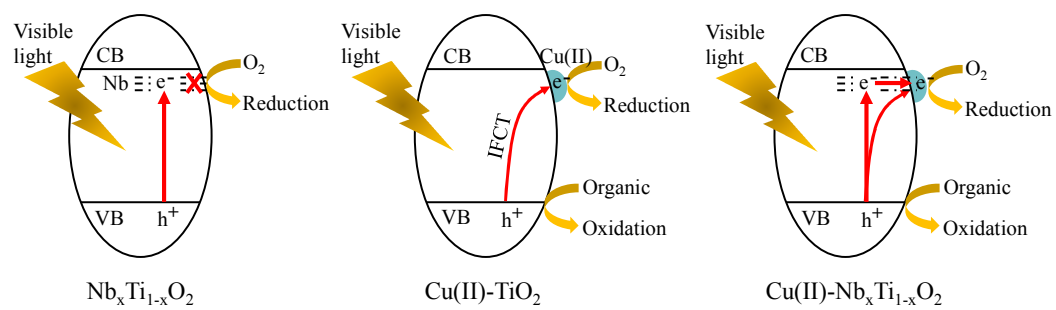


Figure 2.

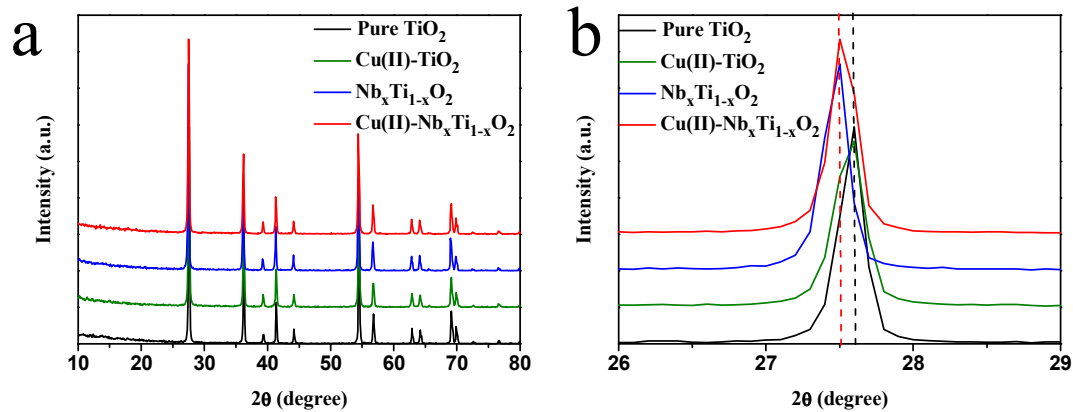




Figure 3

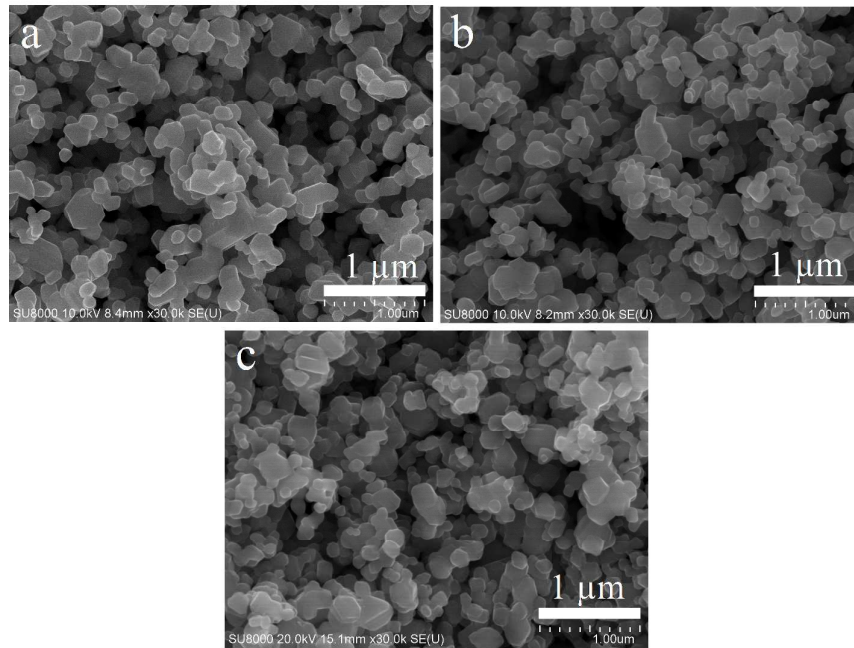


Figure 4.

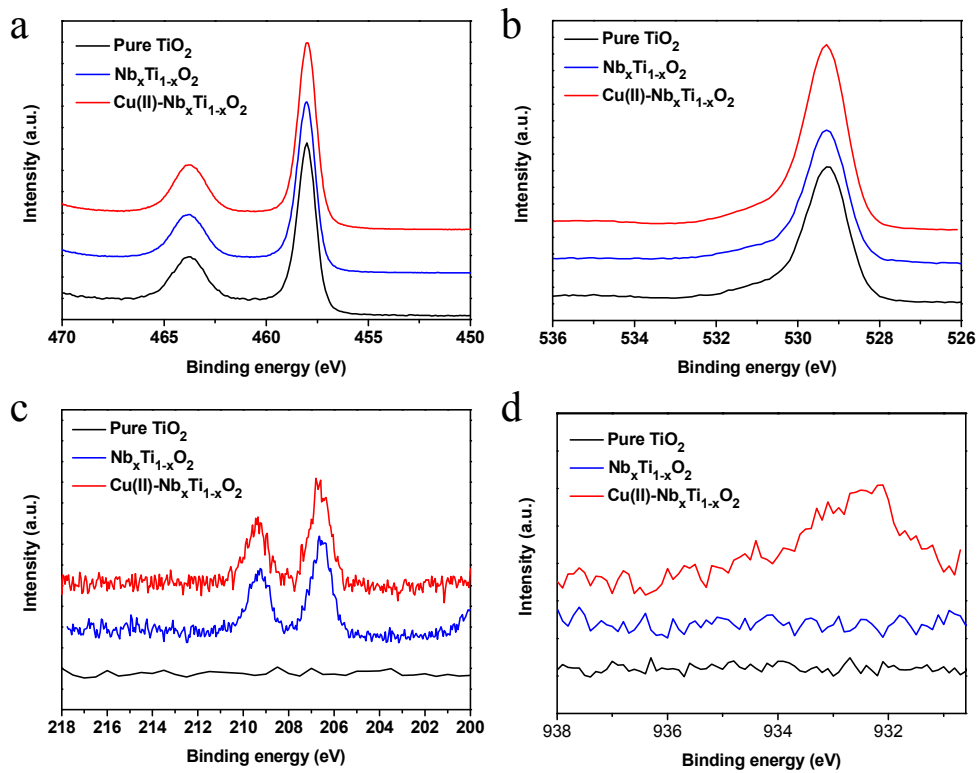


Figure 5.

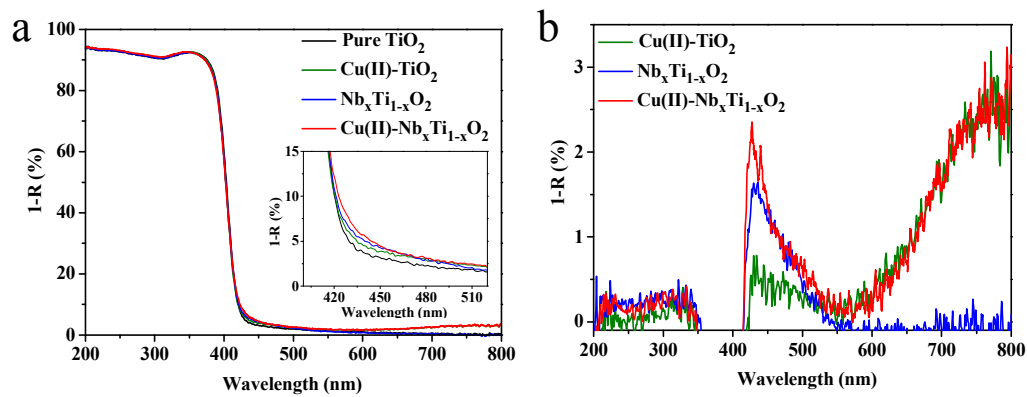
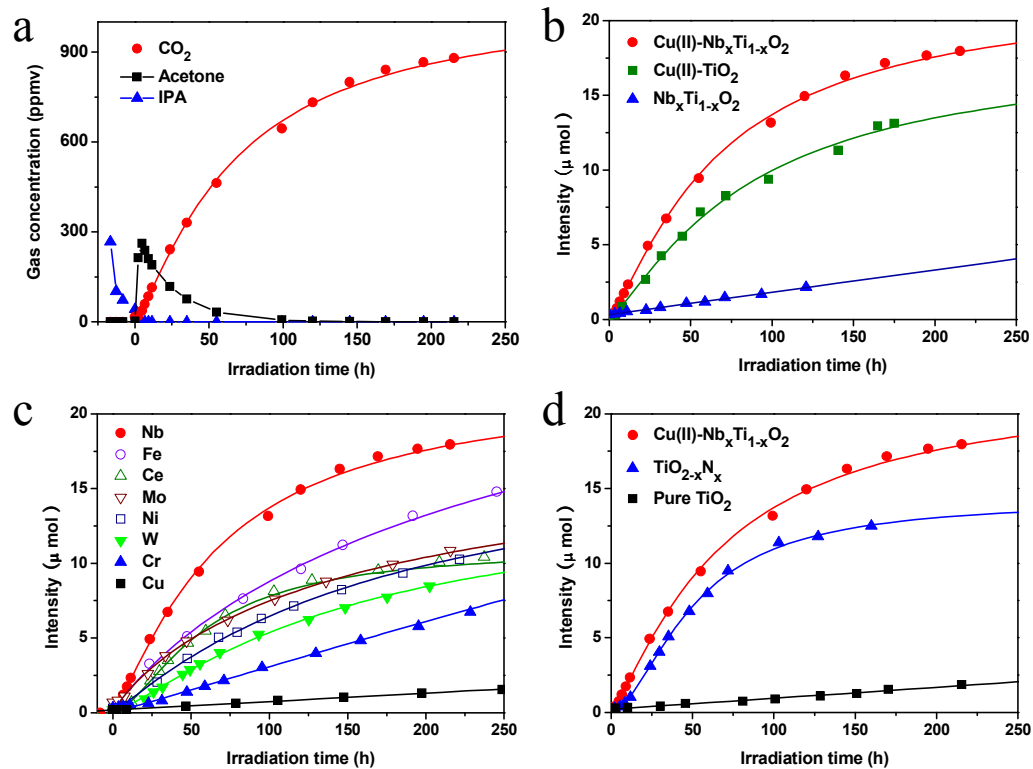


Figure 6.



## Table of contents

Efficient visible-light-sensitive  $\text{TiO}_2$  photocatalysts were developed based on the energy level matching between surface-grafted Cu(II) nanoclusters and bulk-doped Nb ions.

